# Insights into the mechanism of action of the chlorophyll derivative $13\text{-}^2\text{-}hydroxypheophytine\ a$ on reducing neutral lipid reserves in zebrafish larvae and mice adipocytes

Ana Carrasco del Amor [a], Rene Hernandez Bautista [b], Siegfried Ussar [b], Susana Cristobal [a,c], Ralph Urbatzka [d,*]

[a] Department of Biomedical and Clinical Sciences, Cell Biology, Faculty of Medicine, Linköping University, SE-58185, Linköping, Sweden
[b] RG Adipocyte and Metabolism, Institute for Diabetes and Obesity, Helmholtz Center Munich, 85764, Neuherberg, Germany
[c] Ikerbasque, Basque Foundation for Sciences, Department of Physiology, Faculty of Medicine, and Nursing, University of the Basque Country UPV/EHU, Spain
[d] Interdisciplinary Centre of Marine and Environmental Research (CIIMAR/CIMAR), University of Porto, Avenida General Norton de Matos, s/n, 4450-208, Matosinhos, Portugal

## ARTICLE INFO

## ABSTRACT

Obesity is a worldwide epidemic and natural products may hold promise in its treatment. The chlorophyll derivative $13\text{-}^2\text{-}hydroxypheophytine$ (*hpa*) was isolated in a screen with zebrafish larvae to identify lipid reducing molecules from cyanobacteria. However, the mechanisms underlying the lipid-reducing effects of *hpa* in zebrafish larvae remain poorly understood. Thus, investigating the mechanism of action of *hpa* and validation in other model organisms such as mice represents important initial steps.

In this study, we identified 14 protein targets of *hpa* in zebrafish larvae by thermal proteome profiling, and selected two targets (malate dehydrogenase and pyruvate kinase) involved in cellular metabolism for further validation by enzymatic measurements. Our findings revealed a dose-dependent inhibition of pyruvate kinase by *hpa* exposure using protein extracts of zebrafish larvae *in vitro,* and in exposure experiments from 3 to 5 days post fertilization *in vivo*. Analysis of untargeted metabolomics of zebrafish larvae detected 940 mass peaks (66 increased, 129 decreased) and revealed that *hpa* induced the formation of various phospholipid species (phosphoinositol, phosphoethanolamine, phosphatidic acid). Inter-species validation showed that brown adipocytes exposed to *hpa* significantly reduced the size of lipid droplets, increased maximal mitochondrial respiratory capacity, and the expression of PPARy during adipocyte differentiation.

In line with our data, previous work described that reduced pyruvate kinase activity lowered hepatic lipid content via reduced pyruvate and citrate, and improved mitochondrial function via phospholipids. Thus, our data provide new insights into the molecular mechanism underlying the lipid reducing activities of *hpa* in zebrafish larvae, and species overlapping functions in reduction of lipids.

## 1. Introduction

Obesity is one of the huge societal challenges. The rate of obesity is increasing worldwide, and data from the World Health Organization show that 650 million people are classified as obese, corresponding to 13% of the world population (WHO, 2021). Obesity is a recognized risk factor for many other diseases, such as diabetes, fatty liver disease, arteriosclerosis and others. A healthy diet and increase of physical exercise is recommended for the prevention of obesity, while pharmacological drugs or bariatric surgery are among the available treatment options (Castro et al., 2016).

Natural products occupy a different chemical space compared to synthetic compounds and add novel chemical diversity to the drug discovery process (Gerwick and Moore, 2012). Cyanobacteria are a very prolific group of photosynthetic microorganisms, and six drugs from cyanobacteria were already approved by the US Food and Drug Administration for the treatment of different tumors (Mayer, 2021). Regarding beneficial activities for metabolic diseases, dietary

supplementation with *Spirulina* improved hyperlipidemic profiles in humans, in particular if combined with exercise (Hernández-Lepe et al., 2019). Yoshinone A was isolated from *Leptolyngbia* sp and reduced triglycerides in 3T3L1 adipocytes *in vitro* and in adipose tissue of high-fat diet induced obese mice *in vivo* (Koyama et al., 2016). Our own bioactivity screenings of cyanobacteria identified several strains, which reduced neutral lipid reservoirs in zebrafish larvae, lipid droplets in fatty-acid overloaded human hepatocytes (Costa et al., 2019), or inhibited intestinal lipid absorption (Bellver et al., 2021). The chlorophyll derivative 13-$^2$-hydroxypheophytine a (*hpa*) was successfully isolated from a marine cyanobacterium with lipid reducing activity and an $EC_{50}$ value of 9 μM (Freitas et al., 2019). The presence of *hpa* was demonstrated in *Spirulina* at high quantity, which may enable the development of a future nutraceutical, since this species is approved for human food consumption (Freitas et al., 2019).

Understanding the mechanism of action of chemicals derived from phenotypic screening assays starts by identifying the proteins in cells that are the direct interactors. A proteome-wide screening for direct protein targets of chemicals was achieved by using mass spectrometry to analyze the thermal shift of the proteins, which is described in the protocols for thermal proteome profiling, and proteome integral solubility alteration (Gaetani et al., 2019; Savitski et al., 2014). We have added modifications to the protocol of thermal proteome profiling for its application to novel bioactive compounds, and identified a list of protein targets from *hpa* in the human hepatocarcinoma cell line HepG2, explaining partially its beneficial effects on obesity and diabetes (Carrasco Del Amor et al., 2019).

The aim of this study was to identify the protein targets of *hpa* in zebrafish larvae by thermal proteome profiling as the first step to predict the mechanism of actions. Following, two identified protein targets, malate dehydrogenase and pyruvate kinase, were analyzed together with the metabolome response in zebrafish. As cross-species validation, mitochondrial respiration, mRNA expression of target genes, and the formation of lipid droplets were evaluated in adipocytes differentiated from mouse brown preadipocytes. The presented data provide important mechanistic insights, how the chlorophyll derivative *hpa* reduces the neutral lipid reserves in zebrafish larvae and mouse adipocytes.

## 2. Material and methods

### 2.1. Bioactive thermal proteome profiling

Zebrafish embryos 5 days post fertilization (DPF) were suspended in a buffer containing 20 mM Tris-HCl and 20 mM sodium chloride (NaCl), at pH 8.5, and mechanically homogenized using a TissueLyser (Qiagen) for 3 min (min) at 25 Hz. The cells were lysed by sonication in cycles of 10 s (sec)/5 s for 3 min at 6–10 μm amplitude at 50% intensity from an exponential ultrasonic horn of 3 mm in a Soniprep 150 MSE (MSE Ltd., Lower Sydenham, London, UK). The insoluble parts were sedimented by centrifugation at 100,000g for 60 min at 4 °C (Carrasco Del Amor et al., 2019), and the protein concentration was determined by BCA assay (Smith et al., 1985). The soluble proteome was used to perform the bioactive thermal proteome profiling assay. The experiment was performed as described in Franken et al. (2015) with some modifications. The soluble proteome at 1 μg/μl was incubated with the studied bioactive compound, *hpa* at 7.5 μg/ml or with dimethyl sulfoxide (DMSO) as solvent control. The samples were incubated for 10 min at 25 °C, divided into 7 aliquots of 100 μl and transferred into 0.2-ml polymerase chain reaction tubes. Independent thermal shift assays were performed at the seven temperatures: 37, 42, 47, 52, 57, 62 and 67 °C. The samples were heated for 3 min followed by 3 min at room temperature. Subsequently, the samples were centrifuged at 100,000 g for 20 min at 4 °C to collect the supernatant proteins that did not alter their solubility. The supernatants were analyzed by label-free nano liquid chromatography-tandem mass spectrometry analysis (nLC-MS/MS) to analyze alterations in the proteome solubility.

### 2.2. Filter aided sample preparation (FASP)

Protein samples were prepared according to Wiśniewski et al. (2009). The protein samples, corresponding to the supernatants after centrifugation, were prepared with SDT buffer (2% SDS, 100 mM Tris-HCl, pH 7.6 and 100 mM DTT). To perform FASP, the samples were diluted with 200 μl of 8 M urea in 0.1 M Tris/HCl, pH 8.5 (UA) in 30 kDa microcon centrifugal filter units, and centrifuged at 14,000 g for 15 min at 20 °C. The concentrated samples were diluted with 200 μl of UA and centrifuged at 14,000 g for 15 min at 20 °C. After discharging the flow-through, 100 μl of 0.05 M iodoacetamide was added to the filter units, mixed for 1 min at 600 rounds per minute (rpm) on a thermo-mixer, and incubated statically for 20 min in dark. The solution was drained by spinning the filter units at 14,000 g for 10 min. The filter units were washed three times with 100 μl buffer UA and centrifuged at 14,000 g for 15 min, and three times with 100 μl of 50 mM ammonium bicarbonate. Endopeptidase trypsin solution in the ratio 1:100 was prepared with 50 mM ammonium bicarbonate, dispensed, and mixed at 600 rpm in the thermomixer for 1 min. These units were then incubated in a wet chamber at 37 °C for about 16 h (h) to achieve effective trypsinization. Following, the filter units were transferred into new collection tubes. To recover the digested peptides, the tubes were centrifuged at 14,000 g for 10 min. Peptide recovery was completed by rinsing the filters with 50 μl of 0.5 M NaCl and centrifugation. The samples were acidified with 10% formic acid (FA) to achieve pH between 3 and 2. The desalting process was performed by reverse phase chromatography in C18 top tips using acetonitrile (ACN; 60% v/v) with FA (0.1% v/v) for elution, and vacuum dried to be stored at −80 °C till further analysis.

### 2.3. Nano LC-MS/MS analysis

The desalted peptides were reconstituted with 0.1% FA in ultra-pure milli-Q water and the concentration was measured using a Nanodrop (Thermo Scientific). Peptides were analyzed in a QExactive quadrupole-orbitrap mass spectrometer (Thermo Scientific). Samples were separated using an EASY nLC 1200 system (Thermo Scientific) and tryptic peptides were injected into a pre-column (Acclaim PepMap 100 Å, 75 μm × 2 cm) and peptide separation was performed using an EASY-Spray C18 reversed-phase nano LC column (PepMap RSLC C18, 2 μm, 100 Å, 75 μm × 25 cm). A linear gradient of 6 to 40% buffer B (0.1% FA in ACN) against buffer A (0.1% FA in water) during 78 min and 100% buffer B against buffer A till 100 min, was carried out with a constant flow rate of 300 nl/min. Full scan MS spectra were recorded in the positive mode electrospray ionization with an ion spray voltage power frequency (pf) of 1.9 kV (kV), a radio frequency lens voltage of 60 and a capillary temperature of 275 °C, at a resolution of 30,000 and top 15 intense ions were selected for MS/MS under an isolation width of 1.2 m/z units. The MS/MS scans with higher energy collision dissociation fragmentation at normalized collision energy of 27% to fragment the ions in the collision induced dissociation mode. Proteome Discoverer (v2.1, Thermo Fischer Scientific) was used for protein identification and quantification. The MS/MS spectra (.raw files) were searched by Sequest HT against Zebrafish database from Uniprot (UP000000437; 46,847 entries). A maximum of 2 tryptic cleavages were allowed, the precursor and fragment mass tolerance were 10 parts per million (ppm) and 0.6 Da, respectively. Peptides with a false discovery rate (FDR) of less than 0.01 and validation based on q-value were used as identified. The minimum peptide length considered was 6 and the FDR was set to 0.1. Proteins were quantified using the average of top three peptide MS1-areas, yielding raw protein abundances. Common contaminants like human keratin and bovine trypsin were also included in the database during the searches for minimizing false identifications. The proteomics data have been deposited in the ProteomeXchange Consortium via the PRIDE partner repository (https://www.ebi.ac.uk/pride/) and the dataset identifier PXD041936.

## 2.4. Analysis of thermal proteome profiling (TPP) experiments

Melting curves were calculated using a sigmoidal fitting approach with the R package TPP, as described in Franken et al. (2015), with modifications. The fold changes were adapted to the 7 temperatures, and the filter criteria for normalization were adjusted to this number of temperatures. The melting curves were fitted after normalization following the equation described, computed in R:

$$f(T) = \frac{1 - plateau}{1 + e^{-\left(\frac{a}{T} - b\right)}} + plateau$$

where T is the temperature, and a, b and "plateau" are constants. The value of f(T) at the lowest temperature Tmin was fixed at 1. The melting point of a protein is defined as the temperature Tm at which half of the amount of the protein has been denatured. The quality criteria for filtering the sigmoidal melting curves were: (i) fitted curves for both vehicle- and compound-treated conditions had an $R^2$ of $>0.8$; (ii) the vehicle curve had a plateau of $<0.3$; (iii) the melting point differences under both the control and the treatment conditions were greater than the melting point difference between the two controls; and (iv) in each biological replicate, the steepest slope of the protein melting curve in the paired set of vehicle- and compound-treated conditions was below $-0.06$. The non-parametric analysis of response curves (NPARC) of the R package was used to detect significant changes in the temperature-dependent melting behavior of each protein due to changes in experimental conditions. The significance threshold was set at $p < 0.05$.

## 2.5. Zebrafish

According to the EC Directive 86/609/EEC for animal experiments, zebrafish larvae in non-independent feeding stages of development are not considered animal experimentation. Wildtype zebrafish (AB strain) were used for production of zebrafish embryos. Fish larvae were raised from 1 to 5 DPF in egg water (60 mg/ml marine salt dis-solved in distilled water) with 20 mM PTU (1-phenyl-2-thiourea) to inhibit melanogenesis at 28 °C in an incubator (VWR). 40 larvae were kept in one petri dish with 20 ml of egg water. 3 DPF zebrafish larvae were transferred to 48-well plates at a density of 8 larvae/well, and exposed during 48h to *hpa* at the final concentration of 7.5 µg/ml and 15 µg/ml. Purity was analyzed by HPLC, HR-ESI-LCMS/MS & $^1$H NRM as described by Freitas et al. (2019). A solvent control (0.1% DMSO) was included in the assays. For enzymatic measurements *in vivo*, 6 wells were used per group (n = 6), while for metabolomics experiments 2 wells were pooled per replicate, and 3 replicates were sampled (n = 3). For enzymatic measurement *in vitro*, 50 larvae were pooled for protein extractions.

## 2.6. Malate dehydrogenase and pyruvate kinase activities

Enzyme activity of malate dehydrogenase and pyruvate kinase was measured in zebrafish larvae in two different experiments. In the first experiment, zebrafish were exposed to *hpa* at 7.5 µg/ml and 15 µg/ml for 48h from 3 DPF to 5 DPF. Zebrafish larvae were homogenized mechanically with beads in the Precellys equipment (Bertin Instruments, USA) at 5550 rpm for 4x 20 s, and centrifuged for 10 min at 17,000g. Supernatant was collected into new Eppendorf tubes, and protein content quantified by the Pierce BCA kit (ThermoFisher, USA). Necessary protein quantity for enzyme activity was tested to be within the range of supplied standards. Activity of enzymes was determined for 20 min at 100 ng per reaction for malate dehydrogenase, and for 30 min at 800 ng for pyruvate kinase using commercial kits (Sigma Aldrich, USA). In the second experiment, a pool of 50 embryos at 5 DPF was processed as described above for protein extraction and quantification. The activity of enzymes was determined for 20 min at 300 ng per reaction for malate dehydrogenase, and for 30 min at 2400 ng for pyruvate kinase. 6

replicates were analyzed for each treatment group (DMSO 0.5%, *hpa* at 7.5 µg/ml and 15 µg/ml).

## 2.7. Zebrafish metabolomics

Metabolites of zebrafish were extracted according to the methodology of Lin et al. (2019) with some modifications. Briefly, samples were homogenized in a Precellys equipment (Bertin Instruments) using RIPA buffer with FMOC-Gly OH (Sigma Aldrich) as an internal standard. Acetone was added, and samples were centrifuged at 17,000g for 10 min at 4 °C. Supernatant was collected and evaporated in a rotavapor until dryness and re-dissolved in a mixture of water/ACN (1:1). Samples were filtered through 0.2 µm filters (Minisart RC 4, Sartorius), transferred to 200 µL vials and stored at -20 °C until analysis. The liquid chromatography high resolution electrospray ionization mass spectrometry (LC–HRESI–MS) was carried out by Orbitrap Exploris 120 Mass Spectrometer (Thermo Scientific) with electrospray ionization (ESI) controlled by Xcalibur 4.4.16.14 and operated in positive mode. A full MS scan with 70,000 FWHM (150 – 2000 m/z range) resolution and data dependent MS2 (ddMS2, Discovery mode) with 17,500 FWHM resolution (3.0 amu was used for isolation window and 35 for normalized collision energy). An ACE UltraCore 2.5 SuperC18 (50 x 2.1 mm; 5 µm ACE® UltraCore, Scotland) column was used. A total injection volume of 5 µL was used for each sample and temperature was kept at 40 °C throughout the procedure. Samples were eluted in a decreasing gradient from 99.5% to 10% of mobile phase A (95% water: 5% methanol: 0.1% FA) and increasing gradient from 0.5% to 90% of mobile phase B (95% isopropanol: 5% methanol: 0.1% FA) for 9.5 min, returning back to the initial condition by 17 min. A flow rate of 0.35 mL·min-1 was used for a total of 20 min. Feature extraction of chromatographic runs were performed with MZmine2 v.2.53 (Pluskal et al., 2010), and parameter are indicated in the Supplementary Table 1 (S1). Data were exported as LCMS peak list for further analyses in MetaboAnalyst (Xia et al., 2009) (https://www.metaboanalyst.ca/home.xhtml). Samples were normalized for the reference feature FMOC-Gly OH and log-transformed. Partial least squares – discriminant analyses (PLS-DA) was performed with the aligned feature list of all three groups with each 3 replicates (DMSO, 7.5 µg/ml hpa, 15 µg/ml hpa). Univariate analyses as fold change analysis, t-tests and volcano plots were performed with the aligned feature list for 2 groups with each 3 replicates. Following, a 3-column table was edited (m.z, p-value, t.score) for analysis of the functional enrichment using the GSEA algorithm, *Danio rerio* as organism, at least 2 entries and p < 0.05 as parameters. 20 metabolites from the volcano plots of DMSO – hpa 15 µg/ml were forwarded for the putative identification of metabolites (top10 2fold change up, top10 2fold change down) using the METLIN database (https://metlin.scripps.edu/) based on the m/z values (MS1 data) and the HMDB human metabolome data base (https://hmdb.ca/). The H-isotopes, ACN, Na$^+$, K$^+$ or other adducts were manually confirmed in the chromatographic runs with the Xcalibur software (ThermoFisher). A feature based molecular networking approach using the GNPS platform (https://gnps.ucsd.edu/ProteoSAFe/static/gnps-splash.jsp) (Wang et al., 2016) was performed following the procedure of Regueiras et al. (2022).

## 2.8. Brown adipocyte differentiation

Brown preadicpocyte B3 clones (BAT B3) were cultured in normal growth medium (DMEM + GlutaMAX, 4.5 g/L D-glucose, pyruvate, 10% fetal bovine serum (FBS) and 1% penicillin/streptomycin). Differentiation of preadicpocytes was induced by adding DMEM containing 10% FBS, 1% penicillin/streptomycin, 500 µM 3-isobutyl-1-methylxanthin/0.5N potassium hydroxide (freshly prepared), 5 µM dexamethasone/100% ethanol, 125 µM indomethacin/DMSO, 1 nM hormone triiodothyronine/0.1% DMSO, 100 nM insulin and 1 µM rosiglitazone to each well (Day 0). After two days, the induction medium was replaced by freshly prepared differentiation medium (DMEM containing 10% FBS,
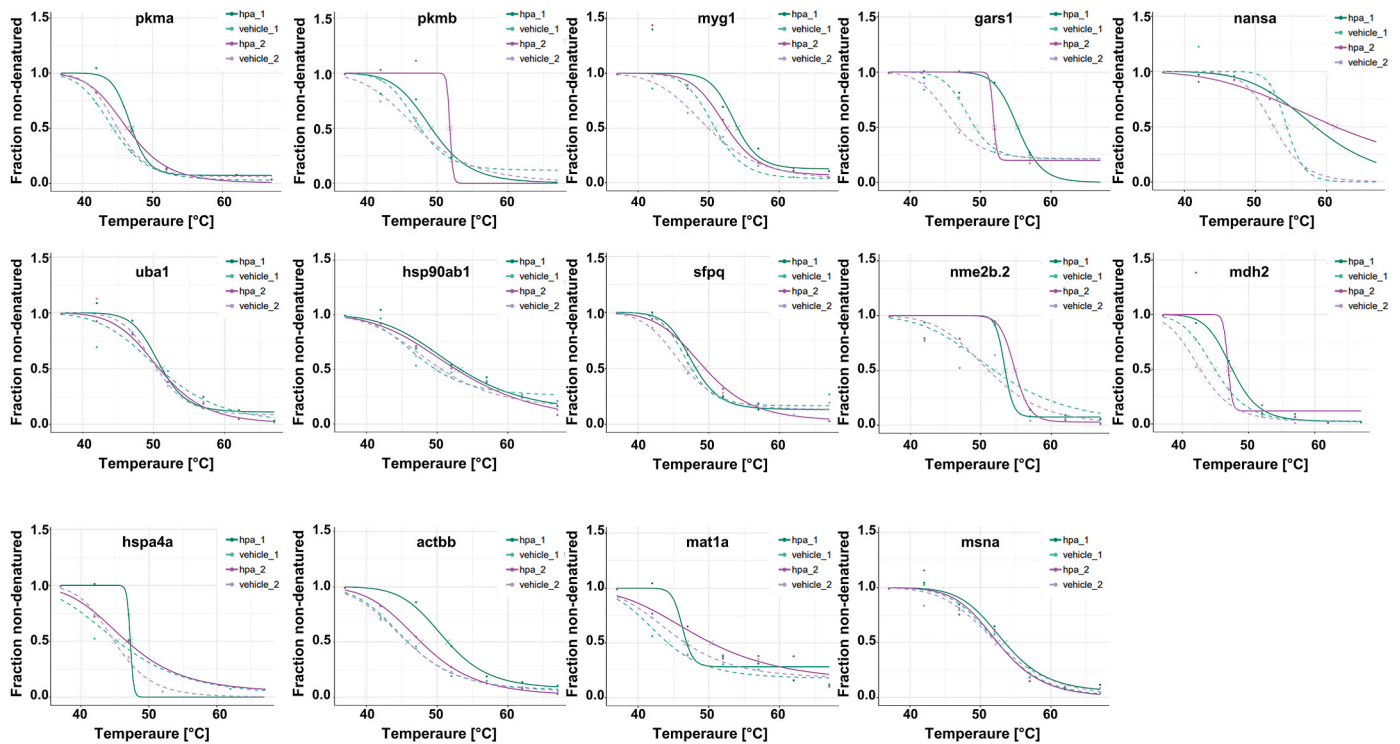
**Fig. 1.** Melting curves of protein targets in response to DMSO (dashed lines) or *hpa* (solid lines) treatment. Protein lysate from zebrafish embryos at 5 DPF was subjected to the thermal shift assay, performed at temperatures between 37 °C and 67 °C, in presence or absence (vehicle) of *hpa*. Melting temperature is shown with an "X" for each melting curve. Two biological replicates were performed.

**Table 1**
Protein targets identified in zebrafish embryo at 5 days post fertilization exposed to *hpa* at 7.5 μg/ml.

| Protein ID | Gene name | Description | Tm Control 1 (°C) | Tm Treatment 1 (°C) | Tm Control 2 (°C) | Tm Treatment 2 (°C) | *p*-value |
|---|---|---|---|---|---|---|---|
| A0A0R4IGP6 | pkma | Pyruvate kinase | 44.39 | 47.04 | 45.07 | 46.39 | 0.217 |
| A0A0R4IHV1 | pkmb | Pyruvate kinase | 47.65 | 49.17 | 47.16 | 51.8 | 0.831 |
| A0A140LG01[a] | myg1 | Melanocyte proliferating gene 1 | 50.88 | 54.1 | 49.91 | 52.61 | 0.006 |
| F1QUV7[a] | gars1 | Glycyl-tRNA synthetase | 49.24 | 55.30 | 46.8 | 51.98 | 0.033 |
| F1R1P6 | nansa | N-acetylneuraminic acid synthase a | 54.40 | 58.38 | 52.57 | 61.24 | 0.754 |
| F1RCA1 | uba1 | Ubiquitin-like modifier-activating enzyme 1 | 50.78 | 51.49 | 45.79 | 47.7 | 0.959 |
| O57521 | hsp90ab1 | Heat shock protein HSP 90-beta | 49.79 | 53.30 | 50.64 | 52.70 | 0.518 |
| Q1L8R2 | sfpq | Splicing factor proline/glutamine-rich | 47.52 | 48.17 | 46.70 | 49.44 | 0.219 |
| Q7SXL4 | nme2b.2 | Nucleoside diphosphate kinase | 51.94 | 53.48 | 51.13 | 54.88 | 0.296 |
| Q7T334[a] | mdh2 | Malate dehydrogenase | 44.88 | 47.51 | 42.65 | 46.92 | 0.018 |
| Q7ZU46 | hspa4a | Heat shock protein 4, like | 45.36 | 47.24 | 44.91 | 46.73 | 0.323 |
| Q7ZVF9[a] | actbb | Actin, cytoplasmic 2 | 45.87 | 51.49 | 45.79 | 47.70 | 0.018 |
| Q7ZW04 | mat1a | S-adenosylmethionine synthase | 44.23 | 46.88 | 46.70 | 50.36 | 0.169 |
| Q66I42 | msna | Moesin a | 52.37 | 53.47 | 52.34 | 52.47 | 0.761 |

[a] Proteins that passed quality criteria and p-value <0.05. Differences in melting temperatures were calculated based on non-parametric analysis of response curves (NPARC).

1% penicillin/streptomycin, 1 nM T3/0.1% DMSO and 100 nM insulin). This medium was changed every other day until the cells were fully differentiated (Day 7-8). Cell cultures were tested regularly negative for mycoplasma contamination. To study the effects of *hpa* on brown adipocyte differentiation and mitochondrial respiration, preadipocytes were differentiated in the presence of 7.5 μg/ml and 15 μg/ml from day 0 until day 2 (induction phase), from day 2 until day 7 (differentiation phase), from day 5 until day 7 (last 48h of differentiation phase) and after day 7 (2h incubation or direct injection into the seahorse cartridge port). DMSO was used as a vehicle and control.

### 2.9. Immunofluorescence and staining of lipid droplets

Standard immunostaining was carried out as previously reported

(Wang et al., 2022). Briefly, after the differentiation phase, the medium was removed, the cells were washed 1x with phosphate buffered saline (PBS) and fixed with 4% paraformaldehyde (PFA)/PBS for 10 min at room temperature. Cells were washed 3x per 5 min with PBS, then washed with PBS/Triton 1%. Cells were blocked for 1h with 3% bovine serum albumin (BSA) in PBS at room temperature, and incubated for 1h with DAPI (Sigma-Aldrich, 1 μg/mL), Alexa Fluor® 546 Phalloidin (Invitrogen™ cat# A22283, 150 nM) and HCS LipidTOX™ Green Neutral Lipid Stain (Invitrogen™ cat# H34775,1:200) diluted in 3% BSA/PBS, in order to stain nucleus, F-Actin and lipids, respectively. The cells were washed with PBS, 0.02% sodium azide was added and samples were stored at 4 °C until imaging. Confocal microscopy was performed using a SP5 confocal microscope (Leica, Heidelberg, Germany), using identical laser intensities and detector gains. Subsequently, images
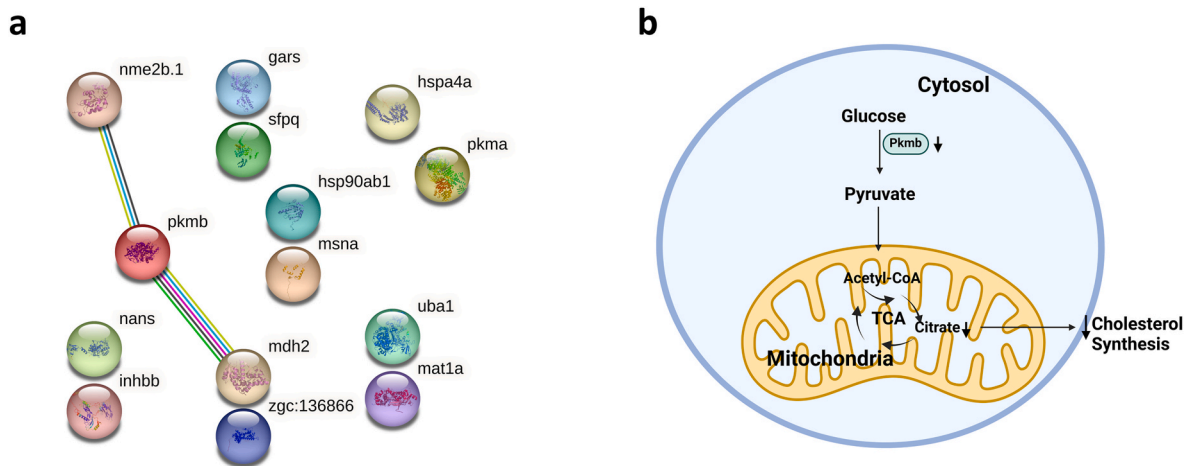
**Fig. 2.** Protein target identification for *hpa* from the soluble proteome of zebrafish embryos. **(a)** String analysis of the protein targets show 3 interactions with highest confidence (score 0.9); **(b)** main protein target and predicted mechanisms of action (Pathway representation were created by Biorender.com).
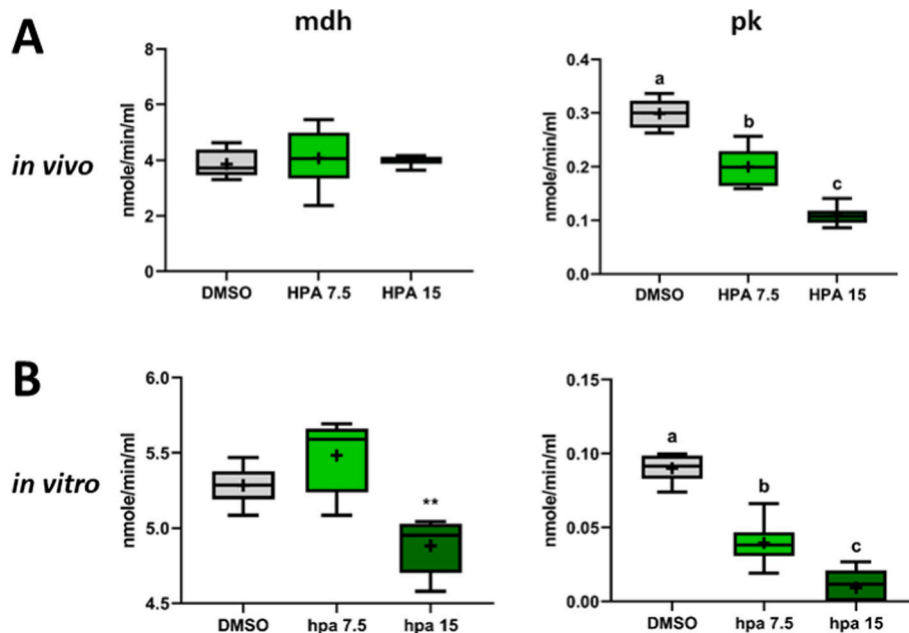


**Fig. 3.** Enzyme activities of malate dehydrogenase (mdh) and pyruvate kinase (pk) in larvae of zebrafish at 5 DPF. a) Larvae were exposed from 3 DPF to 5 DPF to 7.5 μg/ml and 15 μg/ml of *hpa*, before proteins were extracted and enzyme activities determined. b) Proteins of larvae at 5 DPF were extracted and enzyme activities analyzed *in vitro*. Box-whisker plots represent 6 replicates per treatment group, solvent control (dimethyl sulfoxide, DMSO 0.1%), 13-$^2$-hydroxypheophytine a (*hpa*). Statistical differences vs the control group were tested with One-Way ANOVA and Dunnett's posthoc test ($p < 0.05$).

of lipid droplets were analyzed using Image J software. A representative picture of at least three independent experiments is shown.

### 2.10. mRNA expression by real-time PCR

For mRNA expression analyses, RNA from differentiated brown adipocytes was isolated using the QuickExtract RNA extraction kit (Epicentre Biotechnologies), following the manufacturer's instructions. Synthesis of cDNA was performed in a Thermo Cycler by using the high-Capacity cDNA reverse transcription kit (Applied Biosystem, Foster City, CA), according to the manufactures protocol. Real-time PCR with SYBR green was performed using iTaq Universal SYBR® Green Supermix (BIO-RAD, USA) in a CFX384 Touch Real-Time PCR Detection System (BIO-RAD, USA). Relative mRNA expression was calculated after normalization by TATA-binding protein expression. Primer sequences are listed in (Costa et al., 2019). Differential expression levels were calculated via the

ΔΔct method (Pfaffl, 2001).

### 2.11. Cellular respiration in brown adipocytes

Mitochondrial bioenergetics were directly measured in differentiated BAT B3 cells with XF Seahorse technology, as previously described (Pramme-Steinwachs et al., 2017). BAT B3 cells were cultured in normal growth medium (DMEM + GlutaMAX, 4.5 g/L D-glucose, pyruvate, 10% FBS and 1% penicillin/streptomycinPen). Cells were plated at 15,000 cells/well into Seahorse XF24 v7 culture plates (Agilent). The following day, the cells were differentiated in growth medium as described above. Oxygen consumption rates (OCR) in BAT-B3 adipocytes were measured by Seahorse technology at day 7 of differentiation. Cells were washed once with respiration medium (Seahorse XF base medium with 0.5 mM pyruvate, 2.8 mM glucose and 0.2% fatty acid free BSA), supplied with 0.45 ml/well respiration medium and incubated in $CO_2$-less conditions
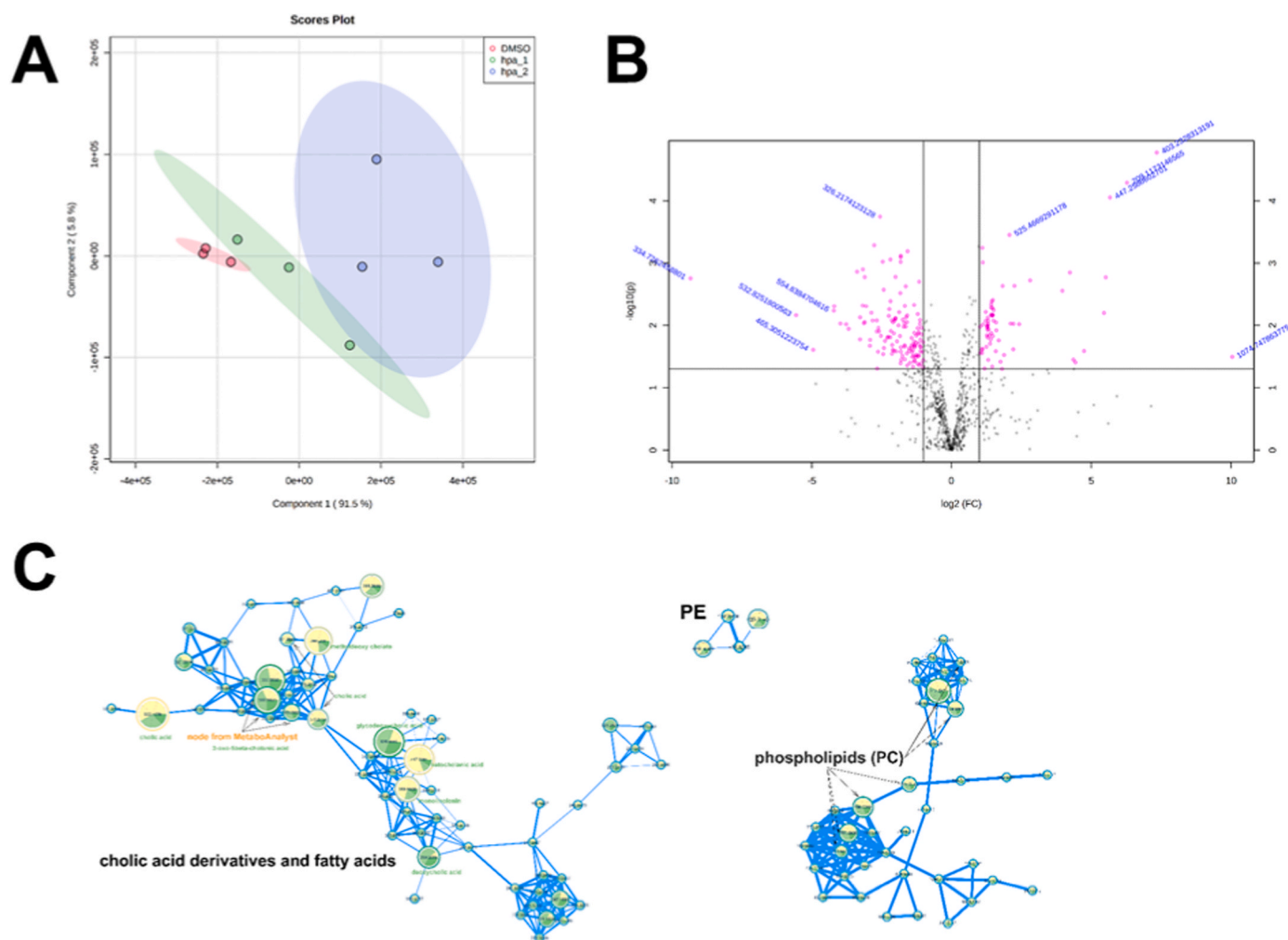
**Fig. 4.** Metabolomics analyses in larvae of zebrafish at 5 DPF. a) PLS-DA plot of larvae exposed from 3 DPF to 5 DPF to *hpa* (DMSO, red; *hpa* 7.5 μg/ml, green; *hpa* 15 μg/ml, blue). b) Vulcano plot of 940 metabolites, indicating the significant different metabolites from the 15 μg/ml *hpa* group vs DMSO. c) Clusters of cholic acid derivatives and fatty acids, phosphoethanolamine (PE) and phosphocholines (PC) identified by feature based molecular networking in GNPS. Bigger nodes represent significant altered metabolites by exposure to 15 μg/ml of *hpa*. Solvent control (dimethylsulfoxide, DMSO 0.1%), 13-[2]-hydroxypheophytine a (*hpa*), log2 FC (log2 fold change).

for 1h.

Equilibrated Seahorse XFe24 cartridges according to the manufacturer were loaded with port injections (75μL/port) to deliver the following drug treatments at final concentrations: oligomycin (0.02 mg/ml), carbonyl cyanide-p-trifluoromethoxyphenylhydrazone (FCCP) (2 μM), rotenone (2.5 μM), antimycin A (2.5 μM) and 2-DG (1M). Four measurements were made under basal conditions and three after each drug injection. Each measurement cycle had the following time parameters: mix 2 min, wait 2 min and measure 2 min. Data are presented as average well OCR (pmol $O_2$/min) at each time point. Error bars represent standard error means (SEM). Basal, proton leak and maximal respiration were computed by subtracting the non-mitochondrial respiration values, represented by the averaged OCR after rotenone/antimycin A/2-DG injection.

### 2.12. Statistics

Experiments from adipocytes were repeated at least three times with triplicate samples. Statistical analysis was performed using Graph Pad Prism and the data are presented as mean ± SEM. Statistical significance was determined by unpaired Student's t-test or, for multiple comparisons by One- or Two-Way ANOVA, followed by Tukey's Multiple Comparison's test. Differences reached statistical significance if p < 0.05.

Results from zebrafish enzyme activities were analyzed for significant differences between the solvent control group and treated groups. Differences were analyzed by One-Way ANOVA followed by Dunnett's test, considering normality and equal variances as assumptions for ANOVA by Kolmogorov-Smirnoff and Bartlett's test, respectively.

### 3. Results

### 3.1. Identification of protein targets from hpa in zebrafish embryos

The identification of proteins interacting with *hpa* was performed by applying bioactive thermal proteome profiling to the proteome from zebrafish embryos at 5 DPF. The concentration of *hpa* was 7.5 μg/ml and the solvent control was DMSO at 0.1%. In the analysis, over 2400 proteins were profiled for changes in thermal folding stability upon interaction with *hpa*, which led to the identification of 14 protein targets (Fig. 1, Table 1). Two proteins were selected for further validation due to its implication in metabolic pathways related to the observed lipid reduction activity in the initial phenotypic screening (Freitas et al., 2019). Additionally, pyruvate kinase and malate dehydrogenase both showed more than 1.5 °C differences between the treatment and the control in the biological replicates, being highly affected by *hpa*. Protein interactions by String analysis were predicted between mdh2, pkmb and

**Table 2**

List of metabolites and their putative identifications that are significant different in zebrafish larvae from 15 μg/ml *hpa* exposure group compared to the solvent control. The 10 most upregulated and 10 most downregulated metabolites were manually searched for putative identifications in the METLIN and HMDB database.

| m/z | log2 FC | p-value | putative identification (m/z; ppm; [ion]) | compound family |
|---|---|---|---|---|
| 1074.748 | 10.041 | 0.032 | - | |
| 403.2328 | 7.3424 | 1.69E-05 | 5S-HETE di-endoperoxide; (403.2332, 0 ppm, [M+H]$^+$) | medium chain fatty acid; metabolite of arachidonic acid |
| 209.1173 | 6.278 | 5.13E-05 | Benzyl (2R,3S)-2-methyl-3-hydroxybutanoate; (209.1172; 0 ppm; [M+H]$^+$) | fatty acid ester; generation of NADPH |
| 447.2589 | 5.6717 | 8.85E-05 | PI(22:2(13Z,16Z)/13:0); (447.2600; 2 ppm; [M+2Na]$^{2+}$) | phospho-inositol |
| 903.5625 | 5.5197 | 0.0017 | PI(18:1(9Z)-O(12,13)/20:2(11Z,14Z)); 903.5593; 4 ppm; [M+H]$^+$) | phospho-inositol |
| 663.4762 | 5.4572 | 0.0063 | PA(14:1(9Z)/22:2(13Z,16Z)); (663.4759; 0 ppm; [M + H-2H2O]$^+$) | phosphatidic acid |
| 893.7205 | 4.7448 | 0.0257 | 22:3-Glc-Sitosterol; (893.7229; 2 ppm; [M+H]$^+$) | sterol lipid/ stigmasterol |
| 895.7359 | 4.4349 | 0.0392 | 22:2-Glc-Sitosterol; (895.7385; 2 ppm; [M+H]$^+$) | sterol lipid/ stigmasterol |
| 375.2794 | 4.3652 | 0.0354 | 3-oxo-5beta-cholanic acid; (357.2794; 0 ppm; M + H-H2O]$^+$) | bile acid |
| 887.5665 | 4.2388 | 0.0014 | PI(20:1(11Z)/18:3(9Z,12Z,15Z)); (887.5664; 2 ppm; [M+H]$^+$) | phospho-inositol |
| 334.7262 | -9.3344 | 0.0017 | - | |
| 532.8252 | -5.5601 | 0.0068 | - | |
| 465.3051 | -4.9504 | 0.0247 | - | |
| 554.8385 | -4.2129 | 0.0058 | - | |
| 475.2079 | -4.1979 | 0.0049 | - | |
| 403.2469 | -3.9761 | 0.0093 | 7α,12α-Dihydroxy-3-oxochola-1,4-dien-24-oic Acid; (403.2479; 2 ppm; [M + H$^+$]) | bile acid |
| 1177.885 | -3.7719 | 0.0096 | - | |
| 417.9222 | -3.6822 | 0.0114 | - | |
| 354.7044 | -3.3805 | 0.0014 | - | |
| 432.5978 | -3.2748 | 0.0168 | - | |

nme2b (Fig. 2a). As depicted in the predicted mechanism, a reduced pkmb activity would lead to less pyruvate and citrate, which could result in reduced lipid or cholesterol synthesis (Fig. 2b). The other targets may also contribute to the cellular responses and observed phenotype through their involvement in molecular pathways that could indirectly alter lipid storage. The S-adenosylmethionine synthase is an enzyme involved in the synthesis of S-adenosylmethionine, a critical molecule for various cellular processes, including methylation reactions and phospholipid synthesis (Dahlhoff et al., 2014).

### 3.2. Enzyme activities

Activity of malate dehydrogenase was not altered by *hpa* treatment when larvae were exposed *in vivo* between 3 DPF and 5 DPF (Fig. 3a). When enzyme activity was measured in protein pools from the zebrafish larvae *in vitro*, a small, but significant reduction of malate dehydrogenase activity was observed in the higher concentration of 15 μg/ml *hpa* (Fig. 3b). In contrast, activity of pyruvate kinase was reduced by *hpa* treatment in a dose-dependent manner in both experiments – exposure

of larvae *in vivo*, and enzyme measurement *in vitro* in a protein pool. It seems reasonable to speculate that pyruvate kinase is the main target of *hpa* exposure in zebrafish larvae.

### 3.3. Zebrafish metabolomics

The partial least square discriminant analysis (PLS-DA) demonstrated that the metabolite profile of the zebrafish from the solvent control group is different from zebrafish derived from 7.5 μg/ml or 15 μg/ml *hpa* exposure groups, and that both *hpa* concentrations clearly differ between them (Fig. 4a). The LCMS/MS dataset was submitted to MassIVE database (https://massive.ucsd.edu/ProteoSAFe/static/massive.jsp) and is accessible under the identifier MSV000092187 and following link: ftp://MSV000092187@massive.ucsd.edu. The functional enrichment analysis in the MetaboAnalyst platform indicated that the exposure to 7.5 μg/ml *hpa* led to the enrichment of the following pathways: C21-steroid hormone biosynthesis and metabolism; arachidonic acid metabolism; androgen and estrogen biosynthesis and metabolism; prostaglandin formation from arachidonate. The exposure to 15 μg/ml *hpa* led to the enrichment of: bile acid biosynthesis; C21-steroid hormone biosynthesis and metabolism; prostaglandin formation from arachidonate; phosphatidylinositol phosphate metabolism; omega-3 fatty acid metabolism. The metabolomics analysis detected 940 metabolites, where 66 (7%) were significantly increased, and 129 (14%) significantly decreased Fig. 4b). The Table 2 shows the putative identifications of the Top10 upregulated and Top10 downregulated metabolites for the 15 μg/ml *hpa* exposure group vs solvent control group. From the 20 metabolites included in the manual search in databases, 12 revealed a putative identification (60%). An increase of various phospholipids species (phosphoinositol, phosphatidic acid), fatty acids and sterol lipids were observed, while bile acids increased or decreased. Interestingly, two mass peaks (663.4762 m/z and 209.1173 m/z), which were putatively identified as PA(14:1(9Z)/22:2(13Z,16Z)) and Benzyl-(2R,3S)-2-methyl-3-hydroxybutanoate, respectively, were also present in the list of the Top10 upregulated metabolites in DMSO vs 7.5 μg/ml, in correspondence to the higher concentration of *hpa*. Additionally, feature based molecular networking was performed on the GNPS platform for zebrafish from the DMSO group vs 15 μg/ml *hpa*. In agreement to the results of the MetaboAnalyst analysis, significantly altered metabolites were identified (p < 0.05 & corr >0.81 or < -0.81) present in a cluster of cholic acid derivatives and fatty acids, and in a cluster of phospholipids as phosphoethanolamines (PE) and phosphocholines (PC) (Fig. 4c),. 3 species of PE (3 significant), 7 species of cholic acid derivatives (5 significant), 6 species of fatty acids (1 significant), and 9 species of PC (2 significant) were identified in those clusters (Supplementary Table 2). The feature based molecular networking for DMSO vs 7.5 μg/ml hpa group identified a cluster of cholic acid derivatives and fatty acids, and a cluster of bile acids, alcohols and derivatives, in correspondence to the results from the higher concentration of *hpa*. 9 species of cholic acid derivatives (4 significant), and 5 species of fatty acids (1 significant) were identified in those clusters (p < 0.05 & corr >0.81 or < -0.81). The mass peak 356.1808 m/z, putatively identified as monolinolein (9c,12c,15c), was significant in both exposure concentrations (Supplementary Table 2).

### 3.4. Hpa bioactivity in brown adipocytes

Brown adipocytes were exposed to *hpa* during differentiation or during the last 48h of the differentiation. We evaluated the possible effect of *hpa* on *de novo* fatty acid biosynthesis by measuring Acetyl-CoA carboxylase 1 (ACACA), sterol regulatory element-binding protein 1c (SREBP-1c) and fatty acid synthase (FAS), one of the main enzymes involved in lipogenesis. The treatment with *hpa* did not appear to directly affect lipid biosynthesis, as indicated by the absence of changes in ACACA and FAS gene expression (Fig. 5a–b). However, increased expression of SREBP-1c was observed when cells were treated with *hpa*
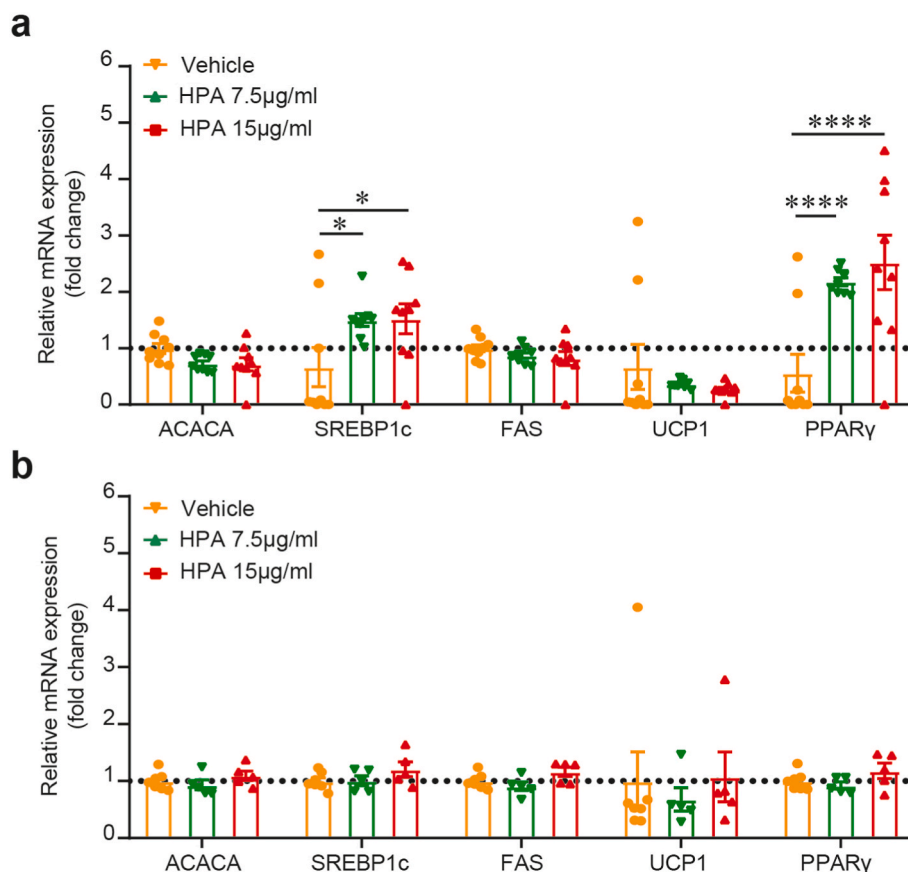
**Fig. 5.** Effects of *hpa* on brown adipocytes. Analysis of mRNA expression of genes involved in lipogenesis (ACACA, SREBP1c and FAS), thermogenesis (UCP1) and adipocyte differentiation (PPARγ) after exposure to *hpa* in the a) differentiation phase and b) last 48h of the differentiation. Values are shown as mean ±SEM. n≥6. Significant differences were analyzed by Two-way ANOVA, followed by Tukey's multiple comparison's test, *p≤0.05, **p≤0.01, ***p≤0.001, ****p≤0.0001.

throughout differentiation, but not when exposed only during the last 48h (Fig. 5a). A key feature of brown adipocytes, compared to white adipocytes is the ability to dissipate energy in form of heat through mitochondrial uncoupling. This process is facilitated through the mitochondrial uncoupling protein 1. We observed a slight, but not significant, downregulation of UCP1 expression when cells were treated with *hpa* throughout the differentiation. This was not observed when cells were exposed to *hpa* only during the last 48h of differentiation (Fig. 5a–b). The impact of *hpa* on adipocyte differentiation per se was assayed by determining the expression of the key adipogenic transcription factor PPARγ. As shown in Fig. 5a, both *hpa* concentrations (7.5 μg/ml, 15 μg/ml) significantly increased PPARγ expression, indicating a possible positive effect on differentiation. No differences compared to control treated cells were found when brown adipocytes were treated only during the last 48h of differentiation (Fig. 5b).

### 3.5. Hpa-treated brown preadipocytes, immunofluorescence images

Quantifications of lipid staining (Fig. 6a) of mature brown adipocytes at day 7 of differentiation showed that cells treated with 15 μg/ml *hpa* had reduced size of lipid droplets. However, treatment with 7.5 μg/ml *hpa* significantly increased the size of lipid droplets (Fig. 6b).

### 3.6. Enhanced mitochondrial respiration in hpa-treated brown adipocytes

A slight, yet statistically significant reduction in basal oxygen consumption was observed in brown adipocytes exposed to 7.5 μg/ml and 15 μg/ml *hpa* compared to the solvent control, when brown adipocytes were exposed to *hpa* during the last 48h of differentiation (Fig. 7). However, this was not observed when cells were chronically exposed to

*hpa*, irrespective of the dose. Oligomycin induced inhibition of ATP-synthase were used to calculate ATP-linked oxygen consumption, which did not show any differences between treatments when adipocytes were treated with *hpa* during the induction phase or throughout differentiation. However, we observed a reduction in ATP-linked oxygen consumption when brown adipocytes were exposed to *hpa* during the last 48h of differentiation. Conversely, maximal respiratory capacity was significantly increased in both dose groups in brown adipocytes when cells were chronically exposed to *hpa*, but not when exposure was restricted to the first or last 48h. Thus, *hpa* appears to affect mitochondrial function in brown adipocytes. However, duration and timing of *hpa* exposure during adipocyte differentiation appear to have a strong impact on the nature of these changes.

## 4. Discussion

Since *hpa* was discovered in a phenotypic screening approach for lipid reduction in zebrafish larvae (Freitas et al., 2019), the molecular mode of action is unknown and needs to be unveiled in additional research efforts. In this study, 14 protein targets were identified in the zebrafish larvae proteome offering the opportunity to explore the mechanism of actions of this recently identified bioactive compound. In particular, malate dehydrogenase and pyruvate kinase were considered relevant, with known roles in cellular metabolism; malate dehydrogenase 2 is a key enzyme of the tricarboxylic acid cycle, contributing to the ATP generation within the mitochondria (Minárik et al., 2002), while pyruvate kinase plays a role in glycolysis and gluconeogenesis (Yamada and Noguchi, 1999). These protein targets match with another study that applied the proteome integral solubility approach in zebrafish larvae, which identified 40 protein interactions with *hpa*, and also
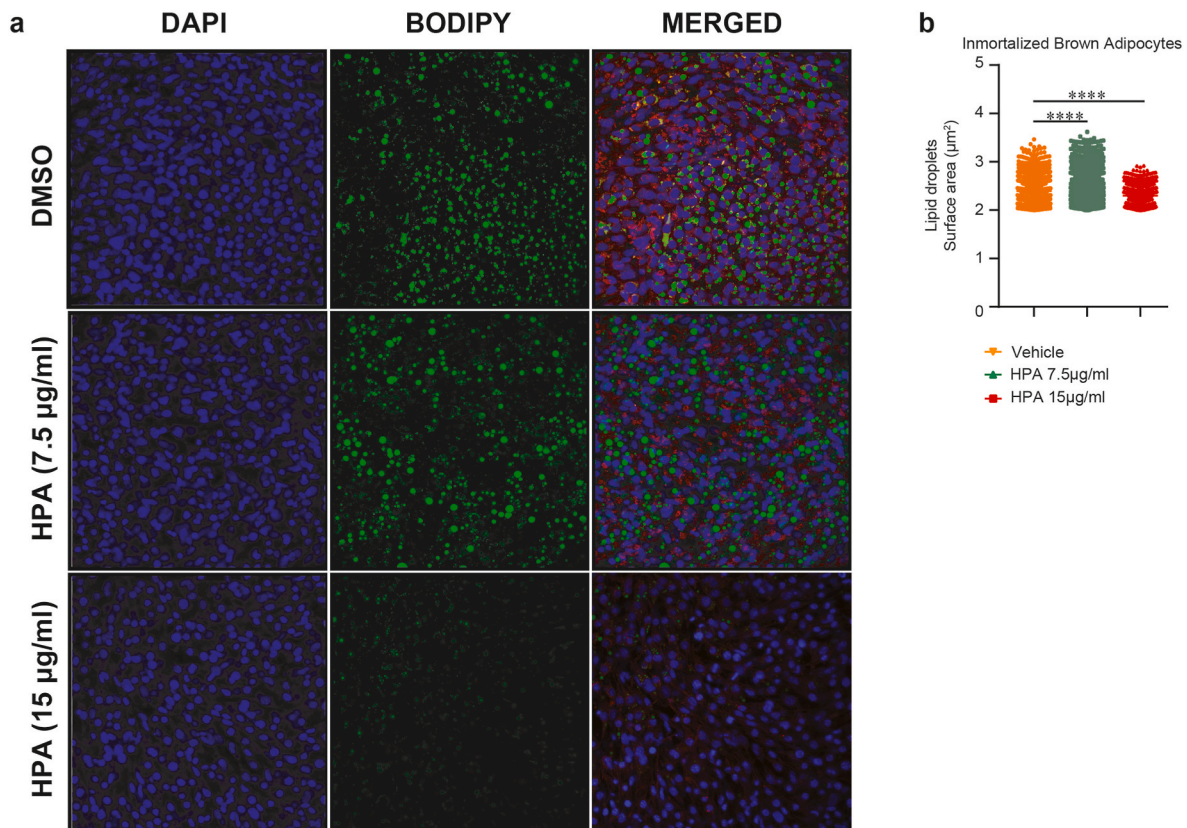
**Fig. 6.** Staining of neutral lipid droplets with BODIPY (493/503) in BAT cells treated with 7.5 μg/ml, and 15 μg/ml of *hpa*. a) Cells stained with BODIPY (green) demonstrate the appearance of spherical lipid droplets within BAT cells, the nucleus (blue) and filamentous actin (red). b) Quantification of the lipid droplets. Statistical differences vs the control group were tested with One-Way ANOVA and Tukey's multiple comparison test (****p < 0.001).

suggested glucose metabolism as affected signaling pathway including the enzyme pyruvate kinase (Lizano-Fallas et al., 2021).

Orthogonal verifications of omics results are important to confirm the findings with other, complementary methodologies. In our case, the confirmation of the proteomics results was done by enzymatic assays in zebrafish, considering two different approaches: exposure of zebrafish larvae *in vivo* to *hpa* between 3 and 5 DPF, and exposure *in vitro* using a protein pool. These experiments confirmed that pyruvate kinase was the main binding protein to *hpa*, since it showed a significant concentration-dependent decrease in both approaches. Pyruvate kinase is one of the rate-limiting enzymes in glycolysis by transferring a phosphate group from PEP to ADP, yielding pyruvate and ATP, and is also involved in the regulation of gluconeogenesis. The reduction of pyruvate kinase activity induces the fasting state and the reduction of energy generation of glycolysis by oxidative phosphorylation; due to intersection to the citric acid cycle, less production of pyruvate yields less citrate, to be used for lipid biogenesis or cholesterol synthesis (Gray et al., 2014). In obese mice, levels of pyruvate kinase are higher than in lean animals, and starvation decreases pyruvate kinase in both (Hron et al., 1984). The difference in pyruvate kinase activity between obese and lean animals might be explained by the hyperinsulinaemia of obese rats, which might lead to the stimulation of glycolysis and lipogenesis (Pérez et al., 1998). Furthermore, pyruvate kinase was shown to be enriched in brown adipocytes, and its silencing caused the up-regulation of *ucp1* mRNA expression, leading to thermogenesis (Isidor et al., 2020). In a system genetic approach, liver pyruvate kinase was analyzed as potential driver for steatosis in mice models and human patients (Chella Krishnan et al., 2021). The silencing in male mice improved glucose tolerance, and insulin sensitivity compared with controls, while reduced plasma cholesterol levels and intrahepatic triglyceride accumulation were observed. Mechanistically, liver pyruvate kinase altered mitochondrial pyruvate flux and its incorporation into citrate. The silencing reduced *de novo* lipogenesis and improved mitochondrial function (Chella Krishnan et al., 2021).

In agreement to the reduced neutral lipid reservoirs by *hpa* exposure in zebrafish larvae (Freitas et al., 2019), the *hpa* exposure in our study led to a decrease in lipid droplet size in brown adipocytes. Additionally, our experiments revealed an increase of the maximum respiratory capacity of mitochondria, a parameter of mitochondrial function, which is seen as a proxy to a metabolic challenge increasing the oxidation of substrates (sugars, fats, amino acids). Interestingly, bilayer forming (PC, PI, PS) and non-bilayer forming (PE, CL) phospholipids are described to affect the activity and stability of respiratory chain supercomplexes, and the function of the mitochondrial membrane architecture, protein import, respiratory metabolism and mitochondrial dynamics (Mårtensson et al., 2017). Concordantly, the analysis of the metabolome of zebrafish larvae exposed to *hpa* in this study revealed the increase of various phospholipid species (PC, PI, PE, PA). The functional enrichment of metabolomics data pointed to arachidonic acid and prostaglandin formation, which besides involvement in various functions can lead to lipid mobilization (Zhuang et al., 2017) or lipolysis in white adipose tissue (Inazumi et al., 2020). Interestingly, dietary polyunsaturated fatty acids, as arachidonic (20:4, omega 6) and eicosapentaenoic (20:5, omega 3) acid, were shown to inhibit hepatic pyruvate kinase (Liimatta et al., 1994).

Malate dehydrogenase 2 was additionally identified as a potential target protein of *hpa* in this study, however, its enzyme activity was regulated to a much lesser content, compared to pyruvate kinase. But this enzyme could also be theoretically involved in the reduction of neutral lipids. In a feeding experiment with mice using a high-fat diet, the substitution of 50% fat by fish oil led to the reduction of body weight and epididymal fat mass (Liu et al., 2021). The omega-3 polyunsaturated
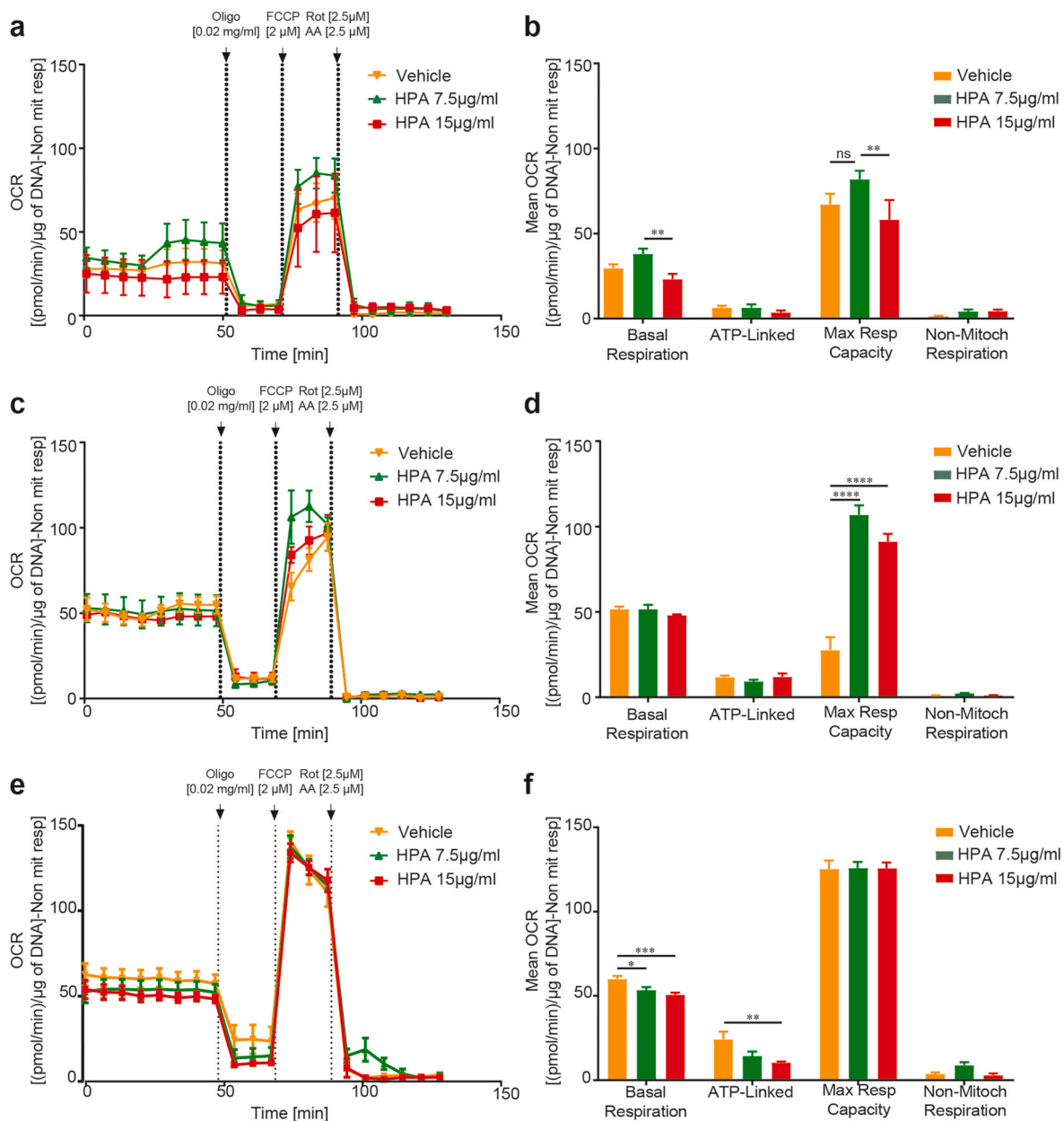
**Fig. 7.** Mitochondrial respiration in BAT B3 cells treated with 13-$^2$-hydroxypheophytin a (*hpa*). Oxygen Consumption Rate (OCR) was detected in controls (vehicle = DMSO) and cells treated with *hpa* (7.5 µg/ml, 15 µg/ml during the induction phase (**a, b**), differentiation phase (**c, d**) or during the last 48hrs of the differentiation phase (**e, f**) under basal conditions or following the addition of oligomycin (0.02 µM), the uncoupling agent FCCP (2 µM) or the electron transport inhibitor rotenone (Rot, 2.5 µM), antymicin A (AA, 2.5 µM) (n = 3). The rates of basal respiration, ATP-linked respiration, maximal respiratory capacity and non-mitochondrial respiration were quantified by normalization of OCR level to the non-mitochondrial respiration. *$p < 0.05$, compared to each non-treated group of BAT B3 cells, analyzed by Two-way ANOVA, followed by Tukey's multiple comparison's test.

fatty acids from the fish oil were suggested to enhance the mitochondrial function *in vivo* and *in vitro*, by reducing the transcription and translation of enzymes from the tricarboxylic acid cycle, including malate dehydrogenase2. Another possible identified target protein for *hpa* was S-adenosylmethionine synthase (*mat1a*), which is an enzyme involved in the synthesis of S-adenosylmethionine (SAM), a critical molecule for various cellular processes, including methylation reactions and phospholipid synthesis (Dahlhoff et al., 2014). Methyl-donor-supplementation was demonstrated to improve fatty liver disease states, eventually by restoring a repression of phosphatidylcholine biosynthesis. Interestingly, *mat1a* deficiency by applying antisense oligonucleotides and genetic depletion in diet-induced obese mice reversed obesity, insulin resistance and hepatosteatosis by increasing

thermogenesis (Sáenz de Urturi et al., 2022).

As comparison to a different species, *hpa* was assessed for their effectiveness on lipid reduction and target gene expression on murine brown adipocytes. Important to note that zebrafish do not possess brown adipose tissue, which is primarily found in mammals and plays a significant role in thermogenesis and energy expenditure. Brown adipocytes contain a high number of mitochondria and specialized uncoupling protein 1 (UCP1), which generates heat by dissipating the energy produced during cellular respiration. Zebrafish have white adipose tissue distributed at various locations on the body, which is responsible for lipid storage, similar to the white adipose tissue in mammals. Interestingly, in the analysis of brown adipocytes in this study, a significant reduction of lipid droplet size was observed, as well as an increase in

PPARy mRNA expression. This is in agreement to the results previously published on zebrafish larvae, where a reduction of neutral lipid reserves and the upregulation of PPARy were described (Freitas et al., 2019). PPARy is involved in adipocyte differentiation, but also has a known role on the distribution of body fat, e.g. on visceral and subcutaneous adipose tissue (Chiarelli and Di Marzio, 2008). The similarity in *hpa* effects on zebrafish larvae and murine brown adipocytes suggest that these effects of *hpa* are independent of species, and provide some evidence that this molecule is also effective in mammals. Future studies should evaluate this aspect in murine pre-clinical models *in vivo*.

Taken those analyses together, the following hypothetic model can be drawn. The exposure to *hpa* leads to a reduction of pyruvate kinase activity, which results in a decrease in lipid accumulation. On the one hand, pyruvate kinase inhibition may decrease pyruvate and hence citrate level, leading to reduced *de novo* lipogenesis. On the other hand, different phospholipid species are formed in response to *hpa*, which may have contributed to the increased maximum respiratory capacity in mitochondria, and hence energy metabolism.

## 5. Conclusions

Bioactive thermal proteome profiling resulted in the identification of 14 potential protein targets. The confirmation by enzyme activities *in vitro* and *in vivo*, showed a dose-dependent reduction of pyruvate kinase activity. An increase of different phospholipid species in zebrafish larvae *in vivo* was observed in parallel to an increase of mitochondrial maximum respiratory activity in brown adipocytes *in vitro*. The exposure to the chlorophyll derivative *hpa* decreased the formation of lipid droplets in murine brown adipocytes, and induced the mRNA expression of *ppary*. These effects are consistent with previous data in zebrafish larvae, and suggest species-independent effects on the lipid metabolism.

## CRediT authorship contribution statement

**Ana Carrasco del Amor:** Formal analysis, Investigation, Writing – original draft, Writing – review & editing. **Rene Hernandez Bautista:** Formal analysis, Investigation, Writing – original draft, Writing – review & editing. **Siegfried Ussar:** Conceptualization, Funding acquisition, Resources, Methodology, Supervision, Writing – original draft, Writing – review & editing. **Susana Cristobal:** Conceptualization, Funding acquisition, Resources, Methodology, Supervision, Writing – original draft, Writing – review & editing. **Ralph Urbatzka:** Conceptualization, Formal analysis, Funding acquisition, Investigation, Resources, Methodology, Writing – original draft, Writing – review & editing.

## Declaration of competing interest

The authors declare no conflict of interest.

## Data availability

Data were submitted to public databases, and links are provided in the manuscript.

## Acknowledgment

## Appendix A. Supplementary data

Supplementary data to this article can be found online at https://doi.org/10.1016/j.ejphar.2023.176158.

## References

Bellver, M., Costa, S.L.D., Sanchez, B.A., Vasconcelos, V., Urbatzka, R., 2021. Inhibition of intestinal lipid absorption by cyanobacterial strains in zebrafish larvae. Mar. Drugs 19, 161. https://doi.org/10.3390/md19030161.

Carrasco Del Amor, A., Freitas, S., Urbatzka, R., Fresnedo, O., Cristobal, S., 2019. Application of bioactive thermal proteome profiling to decipher the mechanism of action of the lipid lowering 13(2)-Hydroxy-pheophytin isolated from a marine cyanobacteria. Mar. Drugs 17, 371. https://doi.org/10.3390/md17060371.

Castro, M., Preto, M., Vasconcelos, V., Urbatzka, R., 2016. Obesity: the metabolic disease, advances on drug discovery and natural product research. Curr. Top. Med. Chem. 16, 2577–2604. https://doi.org/10.2174/1568026616666160415155644.

Chella Krishnan, K., Floyd, R.R., Sabir, S., Jayasekera, D.W., Leon-Mimila, P.V., Jones, A. E., Cortez, A.A., Shravah, V., Péterfy, M., Stiles, L., Canizales-Quinteros, S., Divakaruni, A.S., Huertas-Vazquez, A., Lusis, A.J., 2021. Liver pyruvate kinase promotes NAFLD/NASH in both mice and humans in a sex-specific manner. Cell. Mol. Gastroenterol. Hepatol. 11, 389–406. https://doi.org/10.1016/j.jcmgh.2020.09.004.

Chiarelli, F., Di Marzio, D., 2008. Peroxisome proliferator-activated receptor-gamma agonists and diabetes: current evidence and future perspectives. Vasc. Health Risk Manag. 4, 297–304. https://doi.org/10.2147/vhrm.s993.

Costa, M., Rosa, F., Ribeiro, T., Hernandez-Bautista, R., Bonaldo, M., Goncalves Silva, N., Eiriksson, F., Thorsteinsdottir, M., Ussar, S., Urbatzka, R., 2019. Identification of cyanobacterial strains with potential for the treatment of obesity-related Co-morbidities by bioactivity, toxicity evaluation and metabolite profiling. Mar. Drugs 17, 280. https://doi.org/10.3390/md17050280.

Dahlhoff, C., Worsch, S., Sailer, M., Hummel, B.A., Fiamoncini, J., Uebel, K., Obeid, R., Scherling, C., Geisel, J., Bader, B.L., Daniel, H., 2014. Methyl-donor supplementation in obese mice prevents the progression of NAFLD, activates AMPK and decreases acyl-carnitine levels. Mol. Metabol. 3, 565–580. https://doi.org/10.1016/j.molmet.2014.04.010.

Franken, H., Mathieson, T., Childs, D., Sweetman, G.M., Werner, T., Tögel, I., Doce, C., Gade, S., Bantscheff, M., Drewes, G., Reinhard, F.B., Huber, W., Savitski, M.M., 2015. Thermal proteome profiling for unbiased identification of direct and indirect drug targets using multiplexed quantitative mass spectrometry. Nat. Protoc. 10, 1567–1593. https://doi.org/10.1038/nprot.2015.101.

Freitas, S., Silva, N.G., Sousa, M.L., Ribeiro, T., Rosa, F., Leao, P.N., Vasconcelos, V., Reis, M.A., Urbatzka, R., 2019. Chlorophyll derivatives from marine cyanobacteria with lipid-reducing activities. Mar. Drugs 17, 229. https://doi.org/10.3390/md17040229.

Gaetani, M., Sabatier, P., Saei, A.A., Beusch, C.M., Yang, Z., Lundstrom, S.L., Zubarev, R. A., 2019. Proteome integral solubility alteration: a high-throughput proteomics assay for target deconvolution. J. Proteome Res. 18, 4027–4037. https://doi.org/10.1021/acs.jproteome.9b00500.

Gerwick, W.H., Moore, B.S., 2012. Lessons from the past and charting the future of marine natural products drug discovery and chemical biology. Chem. Biol. 19, 85–98. https://doi.org/10.1016/j.chembiol.2011.12.014.

Gray, L.R., Tompkins, S.C., Taylor, E.B., 2014. Regulation of pyruvate metabolism and human disease. Cell. Mol. Life Sci. 71, 2577–2604. https://doi.org/10.1007/s00018-013-1539-2.

Hernández-Lepe, M.A., Wall-Medrano, A., López-Díaz, J.A., Juárez-Oropeza, M.A., Hernández-Torres, R.P., Ramos-Jiménez, A., 2019. Hypolipidemic effect of arthrospira (Spirulina) maxima supplementation and a systematic physical exercise Program in overweight and obese men: a double-blind, randomized, and crossover controlled trial. Mar. Drugs 17, 270. https://doi.org/10.3390/md17050270.

Hron, W.T., Sobocinski, K.A., Menahan, L.A., 1984. Enzyme activities of hepatic glucose utilization in the fed and fasting genetically obese mouse at 4-5 months of age. Horm. Metab. Res. 16, 32–36. https://doi.org/10.1055/s-2007-1014893.

Inazumi, T., Yamada, K., Shirata, N., Sato, H., Taketomi, Y., Morita, K., Hohjoh, H., Tsuchiya, S., Oniki, K., Watanabe, T., Sasaki, Y., Oike, Y., Ogata, Y., Saruwatari, J., Murakami, M., Sugimoto, Y., 2020. Prostaglandin E(2)-EP4 Axis promotes lipolysis and fibrosis in adipose tissue leading to ectopic fat deposition and insulin resistance. Cell Rep. 33, 108265 https://doi.org/10.1016/j.celrep.2020.108265.

Isidor, M.S., Winther, S., Markussen, L.K., Basse, A.L., Quistorff, B., Nedergaard, J., Emanuelli, B., Hansen, J.B., 2020. Pyruvate kinase M2 represses thermogenic gene expression in brown adipocytes. FEBS Lett. 594, 1218–1225. https://doi.org/10.1002/1873-3468.13716.

Koyama, T., Kawazoe, Y., Iwasaki, A., Ohno, O., Suenaga, K., Uemura, D., 2016. Anti-obesity activities of the yoshinone A and the related marine γ-pyrone compounds. J. Antibiot. 69, 348–351. https://doi.org/10.3390/nu14050968.

Liimatta, M., Towle, H.C., Clarke, S., Jump, D.B., 1994. Dietary polyunsaturated fatty acids interfere with the insulin/glucose activation of L-type pyruvate kinase gene

transcription. Mol. Endocrinol. 8, 1147–1153. https://doi.org/10.1210/mend.8.9.7838147.

Lin, Y.C., Huang, C., Huang, H.C., Liao, M.T., Lai, Y.H., 2019. Metabolomics profiling of haloperidol and validation of thromboxane-related signaling in the early development of zebrafish. Biochem. Biophys. Res. Commun. 513, 608–615. https://doi.org/10.1016/j.bbrc.2019.04.003.

Liu, R., Chen, L., Wang, Z., Zheng, X., Hou, Z., Zhao, D., Long, J., Liu, J., 2021. Omega-3 polyunsaturated fatty acids prevent obesity by improving tricarboxylic acid cycle homeostasis. J. Nutr. Biochem. 88, 108503 https://doi.org/10.1016/j.jnutbio.2020.108503.

Lizano-Fallas, V., Carrasco Del Amor, A., Cristobal, S., 2021. Systematic analysis of chemical-protein interactions from zebrafish embryo by proteome-wide thermal shift assay, bridging the gap between molecular interactions and toxicity pathways. J. Proteomics 249, 104382. https://doi.org/10.1016/j.jprot.2021.104382.

Mårtensson, C.U., Doan, K.N., Becker, T., 2017. Effects of lipids on mitochondrial functions. Biochim. Biophys. Acta Mol. Cell Biol. Lipids 1862, 102–113. https://doi.org/10.1016/j.bbalip.2016.06.015.

Mayer, A.M.S., 2021. The Global Marine Pharmaceuticals Pipeline. http://marinepharmacology.org/home. (Accessed 28 October 2022).

Minárik, P., Tomásková, N., Kollárová, M., Antalík, M., 2002. Malate dehydrogenases– structure and function. Gen. Physiol. Biophys. 21, 257–265.

Pérez, J.X., Manzano, A., Tauler, A., Bartrons, R., 1998. Effect of starvation on gene expression of regulatory enzymes of glycolysis/gluconeogenesis in genetically obese (fa/fa) Zucker rats. Int. J. Obes. Relat. Metab. Disord. 22, 667–672. https://doi.org/10.1038/sj.ijo.0800645.

Pfaffl, M.W., 2001. A new mathematical model for relative quantification in real-time RT-PCR. Nucleic Acids Res. 29, e45. https://doi.org/10.1093/nar/29.9.e45.

Pluskal, T., Castillo, S., Villar-Briones, A., Oresic, M., 2010. MZmine 2: modular framework for processing, visualizing, and analyzing mass spectrometry-based molecular profile data. BMC Bioinf. 11, 395. https://doi.org/10.1038/ja.2016.19.

Pramme-Steinwachs, I., Jastroch, M., Ussar, S., 2017. Extracellular calcium modulates brown adipocyte differentiation and identity. Sci. Rep. 7, 8888. https://doi.org/10.1038/ijo.2017.224.

Regueiras, A., Huguet, Á., Conde, T., Couto, D., Domingues, P., Domingues, M.R., Costa, A.M., Silva, J.L.D., Vasconcelos, V., Urbatzka, R., 2022. Potential anti-obesity, anti-steatosis, and anti-inflammatory properties of extracts from the microalgae chlorella vulgaris and chlorococcum amblystomatis under different growth conditions. Mar. Drugs 20, 9. https://doi.org/10.3390/md20010009.

Sáenz de Urturi, D., Buqué, X., Porteiro, B., Folgueira, C., Mora, A., Delgado, T.C., Prieto-Fernández, E., Olaizola, P., Gómez-Santos, B., Apodaka-Biguri, M., González-Romero, F., Nieva-Zuluaga, A., Ruiz de Gauna, M., Goikoetxea-Usandizaga, N., García-Rodríguez, J.L., Gutierrez de Juan, V., Aurrekoetxea, I., Montalvo-Romeral, V., Novoa, E.M., Martín-Guerrero, I., Varela-Rey, M., Bhanot, S., Lee, R., Banales, J.M., Syn, W.K., Sabio, G., Martínez-Chantar, M.L., Nogueiras, R., Aspichueta, P., 2022. Methionine adenosyltransferase 1a antisense oligonucleotides activate the liver-brown adipose tissue axis preventing obesity and associated hepatosteatosis. Nat. Commun. 13, 1096. https://doi.org/10.1038/s41467-022-28749-z.

Savitski, M.M., Reinhard, F.B., Franken, H., Werner, T., Savitski, M.F., Eberhard, D., Martinez Molina, D., Jafari, R., Dovega, R.B., Klaeger, S., Kuster, B., Nordlund, P.,

Bantscheff, M., Drewes, G., 2014. Tracking cancer drugs in living cells by thermal profiling of the proteome. Science 346, 1255784. https://doi.org/10.1126/science.1255784.

Smith, P.K., Krohn, R.I., Hermanson, G.T., Mallia, A.K., Gartner, F.H., Provenzano, M.D., Fujimoto, E.K., Goeke, N.M., Olson, B.J., Klenk, D.C., 1985. Measurement of protein using bicinchoninic acid. Anal. Biochem. 150, 76–85. https://doi.org/10.1016/0003-2697(85)90442-7.

Wang, J., Onogi, Y., Krueger, M., Oeckl, J., Karlina, R., Singh, I., Hauck, S.M., Feederle, R., Li, Y., Ussar, S., 2022. PAT2 regulates vATPase assembly and lysosomal acidification in brown adipocytes. Mol. Metabol. 61, 101508 https://doi.org/10.1016/j.molmet.2022.101508.

Wang, M., Carver, J.J., Phelan, V.V., Sanchez, L.M., Garg, N., Peng, Y., Nguyen, D.D., Watrous, J., Kapono, C.A., Luzzatto-Knaan, T., Porto, C., Bouslimani, A., Melnik, A. V., Meehan, M.J., Liu, W.T., Crüsemann, M., Boudreau, P.D., Esquenazi, E., Sandoval-Calderón, M., Kersten, R.D., Pace, L.A., Quinn, R.A., Duncan, K.R., Hsu, C. C., Floros, D.J., Gavilan, R.G., Kleigrewe, K., Northen, T., Dutton, R.J., Parrot, D., Carlson, E.E., Aigle, B., Michelsen, C.F., Jelsbak, L., Sohlenkamp, C., Pevzner, P., Edlund, A., McLean, J., Piel, J., Murphy, B.T., Gerwick, L., Liaw, C.C., Yang, Y.L., Humpf, H.U., Maansson, M., Keyzers, R.A., Sims, A.C., Johnson, A.R., Sidebottom, A. M., Sedio, B.E., Klitgaard, A., Larson, C.B., Boya P, C.A., Torres-Mendoza, D., Gonzalez, D.J., Silva, D.B., Marques, L.M., Demarque, D.P., Pociute, E., O'Neill, E.C., Briand, E., Helfrich, E.J.N., Granatosky, E.A., Glukhov, E., Ryffel, F., Houson, H., Mohimani, H., Kharbush, J.J., Zeng, Y., Vorholt, J.A., Kurita, K.L., Charusanti, P., McPhail, K.L., Nielsen, K.F., Vuong, L., Elfeki, M., Traxler, M.F., Engene, N., Koyama, N., Vining, O.B., Baric, R., Silva, R.R., Mascuch, S.J., Tomasi, S., Jenkins, S., Macherla, V., Hoffman, T., Agarwal, V., Williams, P.G., Dai, J., Neupane, R., Gurr, J., Rodríguez, A.M.C., Lamsa, A., Zhang, C., Dorrestein, K., Duggan, B.M., Almaliti, J., Allard, P.M., Phapale, P., Nothias, L.F., Alexandrov, T., Litaudon, M., Wolfender, J. L., Kyle, J.E., Metz, T.O., Peryea, T., Nguyen, D.T., VanLeer, D., Shinn, P., Jadhav, A., Müller, R., Waters, K.M., Shi, W., Liu, X., Zhang, L., Knight, R., Jensen, P.R., Palsson, B.O., Pogliano, K., Linington, R.G., Gutiérrez, M., Lopes, N.P., Gerwick, W. H., Moore, B.S., Dorrestein, P.C., Bandeira, N., 2016. Sharing and community curation of mass spectrometry data with global natural products social molecular networking. Nat. Biotechnol. 34, 828–837. https://doi.org/10.1038/nbt.3597.

WHO, World Health Organization, 2021. Fact Sheets: Obesity and Overweight. (Accessed 11 September 2022).

Wiśniewski, J.R., Zougman, A., Nagaraj, N., Mann, M., 2009. Universal sample preparation method for proteome analysis. Nat. Methods 6, 359–362. https://doi.org/10.1038/nmeth.1322.

Xia, J., Psychogios, N., Young, N., Wishart, D.S., 2009. MetaboAnalyst: a web server for metabolomic data analysis and interpretation. Nucleic Acids Res. 37, W652–W660. https://doi.org/10.1186/1471-2105-11-395.

Yamada, K., Noguchi, T., 1999. Nutrient and hormonal regulation of pyruvate kinase gene expression. Biochem. J. 337 (Pt 1), 1–11.

Zhuang, P., Shou, Q., Lu, Y., Wang, G., Qiu, J., Wang, J., He, L., Chen, J., Jiao, J., Zhang, Y., 2017. Arachidonic acid sex-dependently affects obesity through linking gut microbiota-driven inflammation to hypothalamus-adipose-liver axis. Biochim. Biophys. Acta, Mol. Basis Dis. 1863, 2715–2726. https://doi.org/10.1016/j.bbadis.2017.07.003.